URSI GASS 2021, Rome, Italy, 28 August - 4 September 2021

Autothresholding in MUSICAL using non-orthogonal signal-noise separation

Sebastian Acuña and Krishna Agarwal*
Department of Physics and Technology, UiT The Arctic University of Norway, Tromsø, Norway
*krishna.agarwal@uit.no

Multiple Signal Classification (MUSIC) has been approached from signal processing [1, 2] for direction of arrival estimation in radar technology and electromagnetic inverse scattering for super-resolved imaging of point scatterers [3, 4]. Recently, it has been adopted for fluorescence optical microscopy through adapting additional physical properties of the forward problem, being called as MUSIC ALgorithm (or MUSICAL) [5]. However, its practical utility has suffered from the need of the user specifying a threshold heuristically [6, 7, 8]. This heuristic threshold has been a bottleneck of MUSICAL, and its precedent MUSIC in general. Here, we present an elegant and effective solution for removing this bottleneck without significantly modifying the algorithm.

1 Brief introduction to MUSICAL

Fluorescence based super-resolution is cast as an scalar inverse source problem in which each fluorescent molecule is a point source emitting random number of photons in any time interval [9, 8]. If the time interval is small enough ($\sim$ ms in practice), the temporal fluctuations have a sufficiently wide probability distribution. The Green's function arises from the microscope and the camera pixels of the microscope camera serve as the detector pixels [10, 11]. In order to exploit the temporal fluctuations, a microscopy video of the fluorescently labeled biological sample is acquired.

It is well known that the Green's function of the microscope, popularly called the point spread function, is spread over only a few pixels of the camera (say w pixels in any lateral direction) whereas the camera chip set may accommodate several thousand pixels in each direction of the camera plane. This property is exploited by making one sub-video per pixel, such that the sub-video is centered at the pixel, has a spatial span (or window) of w pixles, and contains all the frames over this window. The operations in the following paragraph are performed for rach sub-video independently.

The sub-video is rearranged to form a matrix in which each row represents the intensity at a camera pixel over time and each column represents one image frame of the microscopy video. This matrix served as the multistatic matrix, or the measurement matrix, which is the starting point of the reconstruction using MUSIC [3] or the core of MUSICAL [5]. Singular value decomposition is performed and the orthogonal set of basis vectors $\{\mathbf{u}_i\}$, along with the corresponding singular values $\{s_i\}$ are computed. Then, the indicator function of MUSICAL is computed on a fine-sampled grid of points in the sample plane to compute a super-resolved sub-image corresponding to the sub-video.

After the super-resolved sub-images are computed for all the sub-videos, the sub-images may be super-imposed at the appropriate locations in the initially empty super-resolved image to form the final super-resolved image. The indicator function is specifically designed so that simple super-imposition is sufficient and no complicated image-processing approach for stitching the images is needed. Here, we focus on the indicator functions of MUSIC and MUSICAL, as they are the premise for this work.

2 Conventional indicator functions of MUSIC and MUSICAL

An important difference between MUSIC and MUSICAL is that MUSICAL uses both signal $\mathscr{S}$ and null $\mathscr{N}$ spaces in the indicator function, whereas the original form in MUSIC only exploited the null space only of the measurement. Elaborating on this point, we present the MUSIC and MUSICAL indicator functions below:

$$f_{\text{MUSIC}}(\mathbf{r}) = \left(\frac{1}{\sqrt{\sum_{\mathbf{u}_i \in \mathscr{N}} \|\mathbf{u}_i \cdot \mathbf{g}(\mathbf{r})\|^2}} \right)^{\alpha} \tag{1}$$

$$f_{\text{MUSICAL}}(\mathbf{r}) = \left(\frac{\sqrt{\sum_{\mathbf{u}_i \in \mathscr{S}} \|\mathbf{u}_i \cdot \mathbf{g}(\mathbf{r})\|^2}}{\sqrt{\sum_{\mathbf{u}_i \in \mathscr{N}} \|\mathbf{u}_i \cdot \mathbf{g}(\mathbf{r})\|^2}} \right)^{\alpha} \tag{2}$$

where $\mathbf{r}$ is the test or sampling point in the sample region where presence of point sources is being investigated, $\{\mathbf{u}_i\}$ is the basis set, and $\mathbf{g}(\mathbf{r})$ indicates the green function vector (i.e. the vector containing the measurements at detectors from a hypothetical point source at $\mathbf{r}$), and α is an empirical parameter.

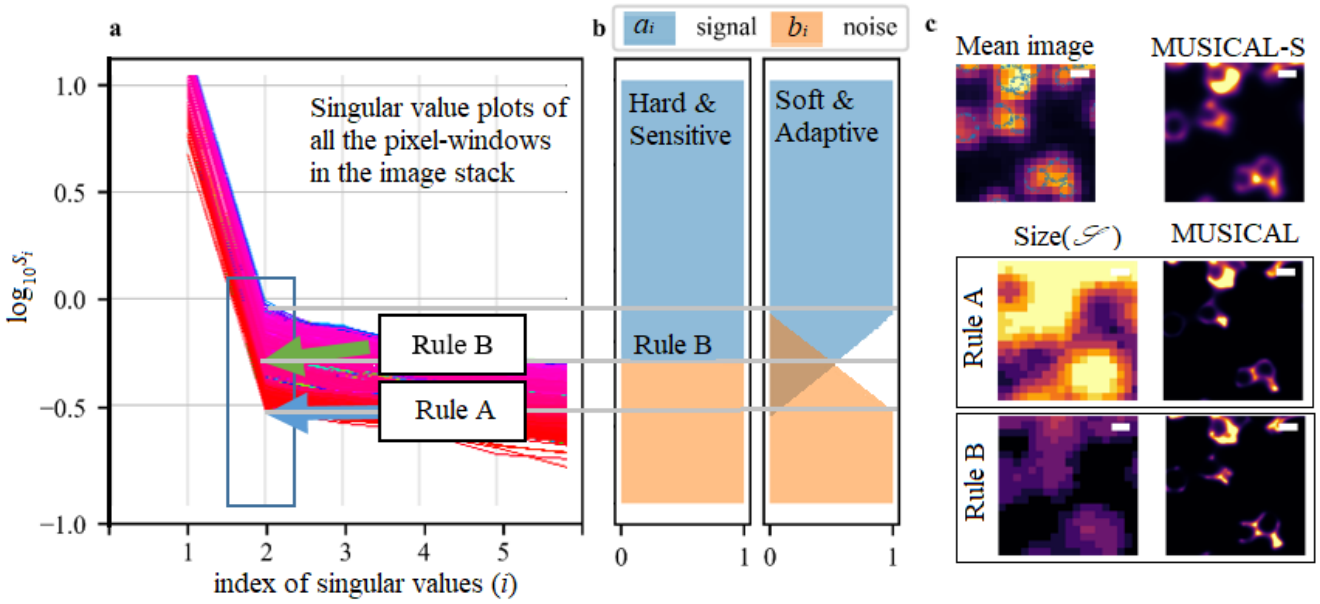

Figure 1. Illustration of the conventional rules for threshold selection are presented in (a). The representation of the conventional hard threshold based indicator function and the soft threshold based redesigned indicator function are illustrated in terms of the coefficient a_i and b_i in eq. 3 is illustrated in (b). The results using hard thresholds (bottom panels) and soft threshold (MUSICAL-S in the top panel) are compared using the mean image (top panel) in (c). The mean image also includes superimposed ground truth structures for reference. The scale bars in (c) are 200 nm each.

Generally, until recently, a user-specified threshold splits the basis set into complementary orthogonal signal and null spaces. The super-resolution in both MUSIC and MUSICAL is derived using the denominator of the indicator function, but is based on an assumption that the null space only represents noise [1, 3, 5]. Furthermore, due to the presence of signal space component in the numerator of the MUSICAL indicator function, the quality of reconstruction also needs that the signal space is not corrupted by noise. However, the choice of threshold quite challenging and subjective [6, 12, 8]. Further, there is no threshold which can reliably split the signal and null spaces so that noise purely affects only the null space, especially if the noise is not additive only. This is a very common trait of noise encountered in microscopy, where beside the additive electronic noise, there is a significant Poisson noise attributed to the photon statistics [13]. Therefore, it is impractical to separate the signal and null spaces strictly in the hope that noise spans only one of them.

3 Soft treatment of signal and null spaces

Recently, a generalized form of MUSICAL indicator function was proposed in [12], as presented below:

$$f_{\text{MUSICAL}}(\mathbf{r}) = \left(\frac{\sqrt{\sum \forall i a_i \|\mathbf{u}_i \cdot \mathbf{g}(\mathbf{r})\|^2}}{\sqrt{\sum \forall i b_i \|\mathbf{u}_i \cdot \mathbf{g}(\mathbf{r})\|^2}} \right)^{\alpha} \tag{3}$$

where a_i and b_i are the weighing coefficients for the contributions of different basis vectors in the numerator and the denominator respectively. MUSIC's indicator function can be thus written as $a_i = \frac{1}{N} \frac{1}{\|\mathbf{u}_i \cdot \mathbf{g}(\mathbf{r})\|^2} \ \forall i$ (equivalent to just fixing to numerator to the constant value 1) and $b_i = 1$ if $\mathbf{u}_i \in \mathscr{N}, 0$ otherwise; and the MUSICAL indicator function as $b_i = 1$ if $\mathbf{u}_i \in \mathscr{N}, 0$ otherwise. In essence, the coefficients in these indicator functions have been binary, incorporating exclusive treatment of the basis vectors used in the numerator and denominator. However, this indeed need not be the case and the generally form allows scope of development of other indicator functions which need not have exclusivity . We considered a simple redesign of the indicator function in which we may include an overlap between the signal and noise subspace. We no longer call the space used in the denominator of the indicator function as the null subspace in order to refrain implying the mathematical property of the null space being orthogonal to the signal space. We also consider that the overlap is along only a few vectors, where the measurement signal and measurement noise are the most comparable and it is difficult to interpret qualitatively or quantitatively the extent to which the basis vectors represent noise. Therefore, we incorporate a fuzzy function to include their contribution in the numerator as well as the denominator. This new function is defined as:

$$a_i = \begin{cases} 1 & \text{if } s_i \geq s_{\text{high}} \\ 0 & \text{if } s_i \leq s_{\text{low}} \\ \frac{\log_{10} s_i - \log_{10} s_{\text{low}}}{\log_{10} s_{\text{high}} - \log_{10} s_{\text{low}}} & \text{otherwise} \end{cases} \tag{4}$$

$$b_i = \begin{cases} 0 & \text{if } s_i \geq s_{\text{high}} \\ 1 & \text{if } s_i \leq s_{\text{low}} \\ \frac{\log_{10} s_{\text{high}} - \log_{10} s_i}{\log_{10} s_{\text{high}} - \log_{10} s_{\text{low}}} & \text{otherwise} \end{cases} \quad (5)$$

where s_i are the singular values associated with the basis vectors, s_{low} and s_{high} are thresholds that define the fuzzy region. The indicator function using the above definition is illustrated comparatively along with the conventional hard threshold mechanism of MUSICAL are illustrated in Fig. 1(b).

4 Autothresholding - sample-adaptive treatment of signal and null spaces

In this section, we present a measurement-derived mechanism to determine s_{low} and s_{high} for the fluorescence microscopy samples. As discussed in section 1, the indicator function is calculated for each sub-video independently. However, a suitable hard threshold for the dataset is chosen by a user visually using a plot such as shown in Fig. 1(a). The singular values of each sub-video (referred to as the pixel-windows in the figure) are plotted using on line plot. All the line plots, one each for one sub-video, are therefore available to the user. In almost all the practical scenarios encountered in the fluorescence data, the knees of the plots occur at the second singular value. Therefore, the user chooses a value of threshold from the range of second singular values seen in the plot. We refer to the range of the second singular values as just 'range' for simplicity. It should not be confused with the range of a matrix as used in linear algebra. The lower bound of the second singular values is recommended as a rule of thumb in the original article, see Rule A in Fig. 1. While it worked well for all the filament like samples used in the paper, later investigations recommended a value in the middle of the range for other biological structures such as mitochondria. See Rule B in Fig. 1. Therefore, even while using the hard threshold, the sample is a factor and the appropriate hard threshold may be different for different samples. Therefore, a proper autothresholding approach has to incorporate sample properties. Here, we take a simple but effective approach. We use the lower and the upper bounds of the range of the second singular values as s_{low} and s_{high}, respectively. We found that it is effective for a wide variety of samples [12].

5 Analysis of the redesigned indicator function

An important consequence of this redesign is that the signal contribution of the measurements utilized in the numerator for stitching are no longer orthogonal to the noise contribution of the measurements utilized in the denominator for super-resolution. We analyze how this property affects the reconstructed super-resolved image by considering the numerator and the denominator sequentially and using the example shown in Fig. 1(c) for illustration.

The basis vectors in the signal space with high singular values are likely to be less corrupted by noise. In the case of a hard threshold, the size of the signal space at each pixel is a function of the threshold rule. Rule A, for example, generally makes the signal space larger for the foreground pixels while Rule B reduces the size of the signal space. This is illustrated in Fig. 1(c). In the case of Rule A, the noisier basis vectors have an equal role as the more reliable vectors. On the other hand, the Rule B discards the signal component in the corrupted basis vectors that are not included in the denominator, and thereby contribute unreliable stitching. Therefore, the stitching performance may be poorer. In the redesigned indicator function, the reliable vectors are retained in their original strength in the numerator, but the more corrupted basis vectors are retained with smaller strengths. This implies that the signal component in them is not completely discarded but the noise component in them is not given an equal chance to compete with less corrupted basis vectors. Therefore, the stitching is expected to be more reliable than using a hard threshold.

Now, consider the denominator that supports super-resolution by allowing the denominator to become miniscule (i.e. tends to zero) at the location of the emitter while remaining finite for the other situations. It does require that the noise space is orthogonal to the signal space. However, such a super-resolution is found not useful in practice, because it makes the value of the indicator function arbitrarily large and contributes a highly non-uniform contrast in the reconstructed image. This effect is evident for both Rules A and B in their MUSICAL images presented in Fig. 1(c). Some low contrast sample details simply drown due to high contrast of the other regions. Therefore, a regularization term in the denominator to deal to stabilize the value of $f(\mathbf{r})$ is quite useful. Indeed, a simple regularization in terms of an additive term may be included but such an approach only opens new questions about suitable regularization and the heuristics related to it. Instead, we introduce regularization through inclusion of the unreliable vectors of the signal space in the denominator, although in diminishing proportions as compared to the vectors which represent mainly the noise. Even at the emitter location, when the original form of the denominator would lead to zero value, the small presence of the signal component makes the denominator non-zero small value. This non-zero small value indirectly restricts the upper limit of the dynamic range of $f(\mathbf{r})$ and therefore regulates the contrast to not vary arbitrarily over the sample region while not deteriorating the resolution of MUSICAL significantly. This is illustrated in the MUSICAL reconstruction using soft threshold (the MUSICAL-S image in Fig. 1(c)) where more sample details are visible in the reconstructed super-resolved image.

6 Discussion and Conclusion

While the work presented here pertains MUSICAL, it can easily be adopted to the conventional MUSIC algorithm for other applications by (a) specifying $a_i = 1$ while using b_i

defined in eq. (5), and (b) determining the practical values of s_{low} and s_{high} for the chosen application. Further, the general form of indicator function may be utilized to design other indicator functions of suitable for specific applications. We will also present open source implementations of MUSICAL so that application scientists from optical microscopy community can use it for diverse bio-applications and scientists from the other domains can adapt it for their specific applications.

Funding

This work was carried out with the funding from the Research Council of Norway's FRIPRO Young fund (288082).

References

[1] R. Schmidt, "Multiple emitter location and signal parameter estimation," IEEE Transactions on Antennas and Propagation **34**, 276–280 (1986).

[2] A. M. Elbir, "Deepmusic: Multiple signal classification via deep learning," arXiv pp. arXiv–1912 (2019).

[3] K. Agarwal and X. Chen, "Applicability of music-type imaging in two-dimensional electromagnetic inverse problems," IEEE Transactions on Antennas and Propagation **56**, 3217–3223 (2008).

[4] K. Agarwal, L. Pan, Y. K. Leong, M. Han, O. Y. Chan, X. Chen, and S. P. Yeo, "Practical applications of multiple signal classification," International Journal of RF and Microwave Computer-Aided Engineering **22**, 359–369 (2012).

[5] K. Agarwal and R. Macháň, "Multiple signal classification algorithm for super-resolution fluorescence microscopy," Nature Communications **7**, 13752 (2016).

[6] S. Acuña, F. Ströhl, I. S. Opstad, B. S. Ahluwalia, and K. Agarwal, "MusiJ: an ImageJ plugin for video nanoscopy," Biomedical Optics Express **11**, 2548–2559 (2020).

[7] S. A. Acuña-Maldonado, "Multiple Signal Classification Algorithm: computational time reduction and pattern recognition applications," Master's thesis, UiT The Arctic University of Norway, Tromsø, Norway (2019).

[8] I. S. Opstad, F. Ströhl, Å. B. Birgisdottir, S. Maldonado, T. Kalstad, T. Myrmel, K. Agarwal, and B. S. Ahluwalia, "Adaptive fluctuation imaging captures rapid subcellular dynamics," in *Advances in Microscopic Imaging II,* vol. 11076 (2019), p. 110761W.

[9] G. T. Dempsey, J. C. Vaughan, K. H. Chen, M. Bates, and X. Zhuang, "Evaluation of fluorophores for optimal performance in localization-based super-resolution imaging," Nature Methods **8**, 1027 (2011).

[10] S. F. Gibson and F. Lanni, "Experimental test of an analytical model of aberration in an oil-immersion objective lens used in three-dimensional light microscopy," Journal of Optical Society of America A **9**, 154–166 (1992).

[11] J. Li, F. Xue, and T. Blu, "Fast and accurate three-dimensional point spread function computation for fluorescence microscopy," Journal of Optical Society of America A **34**, 1029–1034 (2017).

[12] S. Acuña, I. S. Opstad, F. Godtliebsen, B. S. Ahluwalia, and K. Agarwal, "Soft thresholding schemes for multiple signal classification algorithm," Optics Express **28**, 34434–34449 (2020).

[13] M. Hirsch, R. J. Wareham, M. L. Martin-Fernandez, M. P. Hobson, and D. J. Rolfe, "A stochastic model for electron multiplication charge-coupled devices–from theory to practice," PloS one **8**, e53671 (2013).